nature methods

BRIEF COMMUNICATION

https://doi.org/10.1038/s41592-019-0451-6

Thermophoretic trap for single amyloid fibril and protein aggregation studies

Martin Fränzl[1], Tobias Thalheim[1], Juliane Adler[2], Daniel Huster[2], Juliane Posseckardt[3], Michael Mertig[3,4] and Frank Cichos[1*]

The study of the aggregation of soluble proteins into highly ordered, insoluble amyloid fibrils is fundamental for the understanding of neurodegenerative disorders. Here, we present a method for the observation of single amyloid fibrils that allows the investigation of fibril growth, secondary nucleation or fibril breakup that is typically hidden in the average ensemble. Our approach of thermophoretic trapping and rotational diffusion measurements is demonstrated for single $A\beta_{40}$, $A\beta_{42}$ and pyroglutamyl-modified amyloid-β variant ($pGlu_3$-$A\beta_{3-40}$) amyloid fibrils.

The self-organization of individual molecular units into functional or pathological structures is fundamental for life. The aggregation of proteins into fibrillar structures may also yield toxic assemblies that are connected to neurodegenerative disorders[1,2]. In the case of amyloid fibrils, the filaments themselves may be non-toxic but seem to catalyze the formation of pathogenic oligomeric protein aggregates[3] in secondary processes during the nucleation and growth of the fibrillar structures.

A major difficulty in the investigation of protein aggregation and other macromolecular nucleation and growth processes is the heterogeneity of the ensemble studied. Ensembles contain aggregates of different sizes that grow in an unsynchronized way. Single fibril optical microscopy studies[4,5] aim to disentangle the heterogeneous ensemble, but none of those experiments has been able to follow the growth of a freely suspended fibril without the perturbing immobilization at a solid interface[6]. Secondary processes such as fibril branching or fracture have been proposed, but these have never been observed directly[7–9].

Here, we present a method that allows not only the spatial confinement of a single fibril over time periods of several hours in solution without surface immobilization[10,11], but also the observation of a single fibril growth in situ. We show that the rotational diffusion coefficient provides a unique indicator for the growth of fibrils with precision down to ~10 nm. The long observation periods enabled us to identify rare events of fibril fracture visually in the recorded images, as well as in the time traces of the rotational diffusion coefficient, thus confirming directly the existence of secondary processes during the growth of amyloid fibrils.

We enable the observation of single amyloid fibrils over rather long periods of time by using thermophoretic drifts of single molecules and nano-objects in temperature gradients as a result of the temperature-dependent solute–solvent interactions[12–14]. A given temperature gradient ∇T causes a thermophoretic drift of a suspended object at a velocity $\mathbf{v}_T = -D_T \nabla T$ as a result of a variety of physical mechanisms[13]. The strength of this drift is characterized by the thermodiffusion coefficient D_T, which is in most cases found to carry a positive sign. Accordingly, molecules and particles are repelled from the hot regions. In liquids, the thermophoretic drift competes with Brownian motion characterized by the diffusion coefficient D_t, and the Soret coefficient $S_T = D_T/D_t$ is given by their relative strength. Values of S_T in the range $0.01–10\,K^{-1}$ are observed depending on the size and the composition of the object of study.

We designed a temperature field with the help of an optically heated, 10-µm-sized chrome ring deposited on a glass coverslip to provide large temperature gradients at small temperature increments (Fig. 1a and Supplementary Note 1). The chrome structure is heated by a focused laser beam (beam waist $\omega_0 \approx 500$ nm) of 808-nm wavelength, which is rotated by an acousto-optic deflector along the circumference of the ring with a frequency of $f = 100$ Hz (Supplementary Note 2 and Methods). The heat released from the chrome structure creates a time-averaged temperature field in the surrounding liquid film, which is confined to a thickness of about 1 µm by a second glass coverslip (Fig. 1a). The temperature field averaged over the liquid film thickness was obtained from finite-element simulations (Fig. 1b and Supplementary Note 3) and matched to the temperature obtained from reference measurements on the Brownian motion of single polystyrene colloids in water (Supplementary Note 4). The temperature minimum in the center of the structure has a nearly parabolic shape (Fig. 1b). At an incident laser power of $P = 1$ mW, the central temperature is elevated by $\Delta T_{center} = 11.3$ K as compared to the ambient temperature. The temperature contrast from the center to the rim is about $\Delta T_{max} - \Delta T_{center} = 8.9$ K. Both temperature elevations scale linearly with the incident laser power. The temperature gradient in the parabolic region is linear and the trap resembles a harmonic trap in good approximation (Supplementary Notes 3 and 5). As compared to optical tweezers, the temperature profile in the center of the trap is the analog of the intensity in optical tweezers, that is, the potential (see Supplementary Note 5 for details).

The evolution of single thioflavin T (ThT)-stained amyloid fibrils inside the trap is observed by fluorescence microscopy[15] (Fig. 1c, Supplementary Video 1 and Supplementary Note 6). For continuous excitation of ThT, photobleaching is found to be sufficiently weak to allow observation of single fibrils over at least several 10-min periods at a time resolution of $\tau = 30$ ms (see Fig. 1d).

During the observation periods, we have access to the center of mass (COM) position (Fig. 1e) and the in-plane orientation of the fibril (Supplementary Video 2 and Supplementary Note 7) in each frame. COM displacements between subsequent frames (Fig. 1f) in the laboratory frame (Fig. 1g) and the fibril frame (Fig. 1h), as

[1]Peter Debye Institute for Soft Matter Physics, Molecular Nanophotonics Group, Leipzig University, Leipzig, Germany. [2]Institute for Medical Physics and Biophysics, Leipzig University, Leipzig, Germany. [3]Kurt-Schwabe-Institut für Mess- und Sensortechnik e.V. Meinsberg, Waldheim, Germany. [4]Institute for Physical Chemistry, Technische Universität Dresden, Dresden, Germany. *e-mail: cichos@physik.uni-leipzig.de

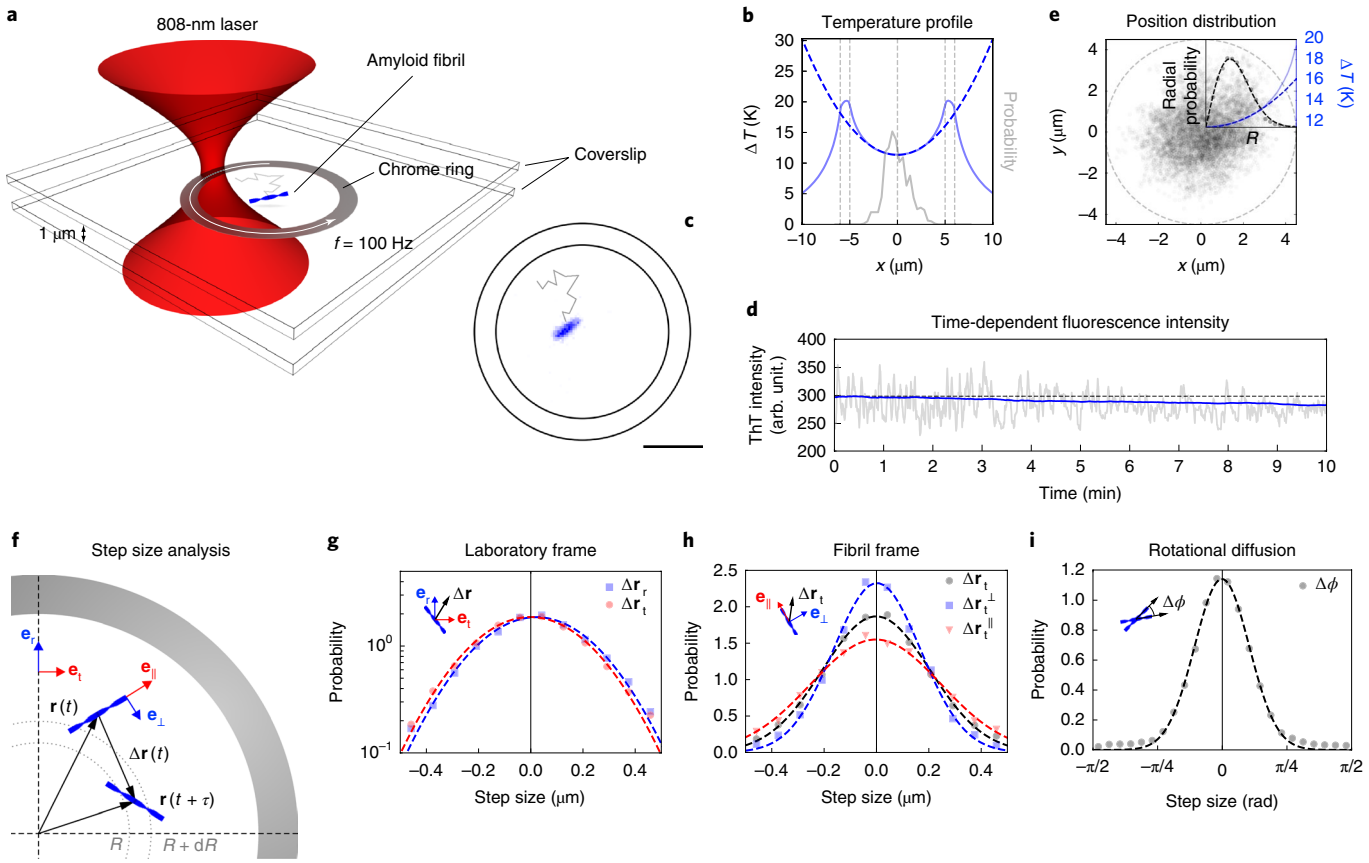

Fig. 1 | Thermophoretic trapping principle and exemplary raw data. a, Illustration of the trapping mechanism and the sample geometry. A chrome ring (10-µm inner diameter, 12-µm outer diameter, 50-nm height) is heated by a focused 808-nm laser rotating along the circumference of the ring at $f = 100$ Hz. **b**, Simulated time-averaged temperature increment $\Delta T(r) = T(r) - T_0$ in the trap ($T_0 = 20$ °C). The temperature profile is averaged over the liquid film thickness of 1 µm and has been matched to the experimentally determined temperature increment in the center of the trap (Supplementary Notes 3 and 4). The dashed blue line represents a parabolic approximation of the temperature profile. The light gray line depicts a line cut through the positional probability density distribution of a trapped single $A\beta_{40}$ fibril ($L = 1.5$ µm) determined from a measurement over a time period of 5 min. These datasets were used in all subsequent panels. **c**, Trapped fibril imaged by the fluorescence of ThT (Supplementary Video 1). A section of the recovered trajectory is depicted in gray. Scale bar, 3 µm. **d**, ThT intensity of a trapped fibril plotted over time. The raw data are shown in gray, and the blue line represents a rolling average. The dashed black line marks the initial intensity value. **e**, Fibril trajectory points recorded over a time period of 5 min. Radial position distribution (inset) determined from the trajectory points and fitted with a Rayleigh distribution (black, dashed line). The distribution is used to calculate the Soret coefficient (Supplementary Note 5). **f**, Sketch showing the decomposition of the fibril displacements $\Delta\mathbf{r}$ according to the laboratory frame (centered at the trap structure) and the fibril frame (fixed in the center of mass of the fibril). **g**, Probability density distribution of $\Delta\mathbf{r}$ projected onto the radial direction $\mathbf{e}_r$ (Δr_r) and tangential direction $\mathbf{e}_t$ (Δr_t) in the trap. The distributions obey Gaussian statistics (dashed lines). The width of the distributions delivers the average translation diffusion coefficient D_t (Supplementary Note 8). The slight displacement of the radial distribution is due to the thermophoretic drift $\mathbf{v}_T$. **h**, Decomposition of $\Delta\mathbf{r}$ along the long axis $\mathbf{e}_\parallel$ ($\Delta r_\parallel$) and short axis $\mathbf{e}_\perp$ ($\Delta r_\perp$) of the fibril. The width of the Gaussian statistics (dashed lines) delivers the projected principle axes of the diffusion tensor ($D_t^\parallel$, $D_t^\perp$) (Supplementary Note 8). **i**, Probability density distribution of angular displacements $\Delta\phi$ of the long axis of the fibril. The experimental data follow Gaussian statistics (dashed line). The width of the Gaussian is used to determine the rotational diffusion coefficient (D_r) (Supplementary Note 8).

well as the angular displacements (Fig. 1i), are used to calculate S_T (Supplementary Note 5), the thermophoretic drift $\mathbf{v}_T$, the diffusion tensor ($D_t^\parallel$, $D_t^\perp$) and the rotational diffusion coefficient D_r (Supplementary Note 8) of the fibril.

We demonstrate the method for single $A\beta_{40}$ fibrils of varying length in an aqueous buffer (pH 8.4, 6 mM NaCl) in the absence of $A\beta_{40}$ peptide monomers (Supplementary Note 9). The fibril length has been estimated from the optical images. Fig. 2a,b displays the obtained length dependence of S_T, the rotational (D_r) and the average translational diffusion coefficient $D_t = (D_t^\parallel + D_t^\perp)/2$ (Supplementary Note 10). The Soret coefficient increases linearly with the length of the fibril (Fig. 2a). The average translation diffusion coefficient D_t follows the inverse linear dependence on the length L and D_r is inversely dependent on the third power of the length ($\propto L^{-3}$) (Supplementary Note 10). The linear dependence of S_T is the result of the inverse dependence of the average translational diffusion coefficient on the length (Fig. 2b). In agreement with the literature[12], the thermodiffusion coefficient is thus independent of the size of the object and found to be $D_T = 1.06\,\mu m^2\,s^{-1}\,K^{-1}$.

Figure 2a,b also includes the corresponding data for $A\beta_{40}$ under varying buffer conditions (pH between 6.1 and 8.8, NaCl concentration between 1 mM and 150 mM, 25 mM phosphate buffer). In all cases, a long trapping time is possible (Supplementary Note 9). The found reduced Soret coefficients S_T/L are similar to the ones obtained for a 6 mM NaCl concentration, highlighting the applicability of the method to a wide range of buffer conditions. Only the highest salt concentration reveals a decreased electrostatic contribution to the Soret coefficient[16]. Other protein fibrils such as a

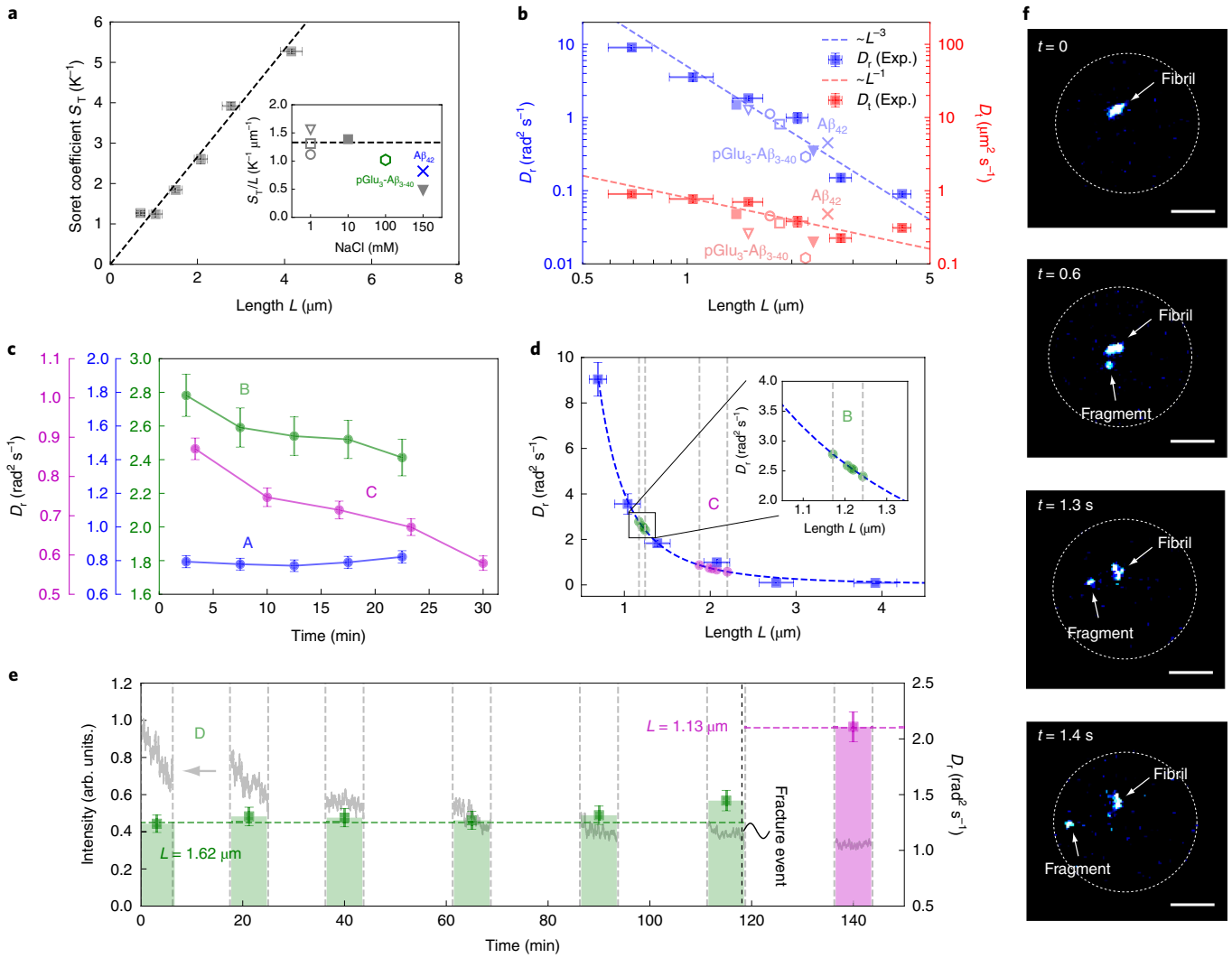

Fig. 2 | Fibril dynamics, growth and breakup. a, Dependence of the Soret coefficient S_T on the fibril length L for $A\beta_{40}$. The line represents the result of a linear regression, which yields a thermodiffusion coefficient of $D_T = 1.06\,\mu m^2\,s^{-1}\,K^{-1}$. Vertical error bars were calculated according to Supplementary Note 12. The horizontal error bars were estimated from the diffraction limit of the setup and the standard deviation of the major axis length. For the sample sizes and buffer conditions, see Supplementary Note 9. The gray symbols in the inset show the reduced Soret coefficient S_T/L for $A\beta_{40}$ for varying salt and pH conditions. The shape of the symbols encodes the pH (circles, pH 6.1; squares, pH 7.4; triangles, pH 8.8). The two additional data points show the results for two different peptides variants: $A\beta_{42}$ (blue cross, pH 9.2) and $pGlu_3$-$A\beta_{3-40}$ (green hexagon, pH 8.0). **b**, Length dependence of the average D_t and D_r for $A\beta_{40}$. The lines display a fit to the experimental data according to the theoretically predicted dependence of the diffusion of a rod ($D_t \propto L^{-1}$, $D_r \propto L^{-3}$, Supplementary Note 10). Vertical error bars for translational/rotational diffusion coefficients are calculated according to Supplementary Note 11. The horizontal error bars were estimated as described in **a**. The measurements on $A\beta_{40}$ for different salt and pH conditions and for the two additional amyloid-forming peptides, $A\beta_{42}$ and $pGlu_3$-Aβ3–40, are represented by the same symbols used in **a**. For the sample sizes and buffer conditions, see Supplementary Note 9. **c**, Time dependence of the rotational diffusion coefficient for three different fibrils ($A\beta_{40}$) in the presence of peptide monomers. The error bars represent the confidence intervals for the statistical sample size and 90% accuracy. Fibril A has a length of 2.1 μm and an initial rotational diffusion coefficient of $D_r = 0.8\,rad^2\,s^{-1}$. The rotational diffusion coefficient is unchanged over a time period of 20 min. Fibril B has a length of 1.2 μm and an initial rotational diffusion coefficient $D_r = 2.8\,rad^2\,s^{-1}$, which shows a continuous decrease attributed to a growth of 70 nm within a time period of 20 min. Fibril C has an initial length of 1.9 μm and a $D_r = 0.88\,rad^2\,s^{-1}$ showing continuous growth by about 300 nm. For the sample sizes and buffer conditions, see Supplementary Note 9. **d**, Data points of fibrils B and C converted to a length according to the measured dependence in **b**. **e**, Maximum intensity of a single fibril D of 1.62-μm length in an intermittent observation scheme. The fluorescence excitation is switched on for time periods of 5 min. The bars indicate the average rotational diffusion coefficient within the observation period. At the end of the sixth observation period, a fibril breakup is observed, which leads in the subsequent period to an increased rotational diffusion coefficient. The change of the rotational diffusion coefficient corresponds to a length change of about 300 nm. **f**, Experimental false color images from the breakup event indicated in **e**. The large fragment of fibril D stays in the trap, while the short segment leaves the trap structure (Supplementary Video 3). Scale bars, 3 μm.

pyroglutamyl-modified Aβ variant ($pGlu_3$-$A\beta_{3-40}$)[17] and $A\beta_{42}$ have been successfully trapped for periods longer than 20 min, and the extracted results seamlessly integrate with the $A\beta_{40}$ data (Fig. 2a,b).

The strong length dependence of D_r delivers an extremely sensitive tool to investigate fibril growth (Supplementary Notes 11 and 12). We monitor the rotational diffusion coefficient of three seed fibrils over time in the presence of $A\beta_{40}$ peptide monomers that enter and leave the trap due to the lower Soret coefficient ($S_T^{peptide} \approx 10^{-2}\,K^{-1}$). Figure 2c shows the time evolution of the rotational diffusion coefficient of two different fibrils (A, B) in the same

sample (pH 8.4, 6 mM NaCl) and a third fibril (C) under high pH and salt (pH 8.8, 150 mM NaCl).

Fibril A appears not to be growing, because of defects at the fibril ends[5]. Fibril B exhibits a decreasing rotational diffusion coefficient. With an initial length of $L = 1.2\,\mu m$, the overall length increase is determined to be 70 nm, which corresponds to a growth rate of $0.06\,nm\,s^{-1}$. Fibril C shows that growth can also be observed under higher pH and salt conditions as encountered in the biological context, which results in a higher growth rate of $0.17\,nm\,s^{-1}$. Figure 2d depicts the measured data points for fibrils B and C in the expected length dependence of the rotational diffusion coefficients together with the data from Fig. 2b. Monitoring of the rotational diffusion is, therefore, an excellent tool for observing fibrillar growth processes in single fibril studies.

The experimentally accessible time for single fibril studies can be extended to several hours because the trapping mechanism does not require an observation of the fibrils as in feedback traps[11,18]. Figure 2e displays the intensity time trace of a single fibril (fibril D) over time periods of 5 min interrupted by periods with no fluorescence excitation. During the first 100 min, no change in the rotational diffusion is detected. At about 118 min, a fibril fracture event is captured on video. A small part breaks off from the fibril and leaves the trap (Fig. 2f and Supplementary Video 3). As a result, the rotational diffusion coefficient shows a sudden increase. The length change has been determined to be about 300 nm and delivers a direct hint for a fracture mechanism as one of the suggested mechanisms of secondary nucleation[2].

The thermophoretic trapping method put forward here provides a starting point for more complex studies of molecular interactions and in particular of protein and macromolecular aggregation processes at the single-fibril level. The rotational diffusion coefficient has been revealed to be a sensitive indicator of growth and can be combined with advanced statistical analysis methods such as change point analysis[19] or wavelet transforms[20] to identify changes. The detection of rotational diffusion is not restricted to rod-like objects and can be extended to polarization resolved fluorescence detection with photodiodes for fast rotational diffusion measurements, although the trapping of very small aggregates or oligomers will be challenging owing to the small Soret coefficients. The trap may be used to access the size distribution of fibrils also by using multiple traps in parallel. Multicolor detection schemes can be introduced to explore surface catalyzed secondary nucleation, and a combination with advanced microfluidics could allow for cross-seeding with different peptides/mutants. Since only relative temperature increments are important for the trapping, the sample temperature can be lowered or increased to provide temperature-dependent measurements of fibrillation processes. Thus, thermophoretic trapping of single amyloid fibrils enables a plethora of applications for the investigation of molecular events that provide the basis for the understanding of diseases related to protein misfolding.

Online content

Any methods, additional references, Nature Research reporting summaries, source data, statements of code and data availability and associated accession codes are available at https://doi.org/10.1038/s41592-019-0451-6.

Received: 3 August 2018; Accepted: 10 May 2019;
Published online: 24 June 2019

References

1. Knowles, T. P. J., Vendruscolo, M. & Dobson, C. M. *Nat. Rev. Mol. Cell Biol.* **15**, 384–396 (2014).
2. Iadanza, M. G., Jackson, M. P., Hewitt, E. W., Ranson, N. A. & Radford, S. E. *Nat. Rev. Mol. Cell Biol.* **19**, 755–773 (2018).
3. Linse, S. *Biophys. Rev.* **9**, 329–338 (2017).
4. Blackley, H. et al. *J. Mol. Biol.* **298**, 833–840 (2000).
5. Pinotsi, D. et al. *Nano Lett.* **14**, 339–345 (2014).
6. Ban, T., Yamaguchi, K. & Goto, Y. *Acc. Chem. Res.* **39**, 663–670 (2006).
7. Tycko, R. *Annu. Rev. Phys. Chem.* **62**, 279–299 (2011).
8. Knowles, T. P. J. et al. *Proc. Natl Acad. Sci. USA* **108**, 14746–14751 (2011).
9. Wolff, M. et al. *Sci. Rep.* **6**, 22829 (2016).
10. Braun, M. & Cichos, F. *ACS Nano* **7**, 11200–11208 (2013).
11. Braun, M., Bregulla, A. P., Günther, K., Mertig, M. & Cichos, F. *Nano Lett.* **15**, 5499–5505 (2015).
12. Piazza, R. & Parola, A. *J. Phys. Condens. Matter* **20**, 153102 (2008).
13. Würger, A. *Rep. Prog. Phys.* **73**, 126601 (2010).
14. Bregulla, A. P., Würger, A., Günther, K., Mertig, M. & Cichos, F. *Phys. Rev. Lett.* **116**, 188303 (2016).
15. Xue, C., Lin, T. Y., Chang, D. & Guo, Z. *R. Soc. Open Sci.* **4**, 160696 (2017).
16. Reichl, M., Herzog, M., Götz, A. & Braun, D. *Phys. Rev. Lett.* **112**, 198101 (2014).
17. Scheidt, H. A., Adler, J., Krueger, M. & Huster, D. *Sci. Rep.* **6**, 1–7 (2016).
18. Cohen, A. E. & Moerner, W. E. *Proc. Natl Acad. Sci. USA* **103**, 4362–4365 (2006).
19. Watkins, L. P. & Yang, H. *J. Phys. Chem. B* **109**, 617–628 (2005).
20. Yang, H. *J. Chem. Phys.* **129**, 074701 (2008).

Acknowledgements

F.C. and D.H. acknowledge financial support by the German Research Foundation (Deutsche Forschungsgemeinschaft, DFG) through the Collaborative Research Center TRR 102 'Polymers under multiple constraints: restricted and controlled molecular order and mobility' (funded by the Deutsche Forschungsgemeinschaft (DFG, German Research Foundation), project number 189853844–SFB TRR 102) and project CI 33/14-1. J.P. and M.M. acknowledge financial support by the BMBF (contract no. 03WKCL01G) and the DFG via the Cluster of Excellence 'cfaed' (contract no. EXC 1056/1). We thank A. Kramer for helping to revise the manuscript.

Author contributions

M.F., T.T. and F.C. designed the experiments. M.F. and T.T. performed the experiments. M.F., T.T. and F.C. analyzed the data. J.A. prepared the amyloid samples and carried out fibrillation kinetics measurements. J.P., M.F., T.T., F.C. and M.M. developed the trap preparation procedure. D.H. and F.C. provided the experimental equipment. M.F., T.T., J.A., D.H. and F.C. wrote the manuscript. All authors discussed the results and commented on the manuscript.

Competing interests

The authors declare no competing interests.

Additional information

Supplementary information is available for this paper at https://doi.org/10.1038/s41592-019-0451-6.

Reprints and permissions information is available at www.nature.com/reprints.

Correspondence and requests for materials should be addressed to F.C.

Peer review information: Allison Doerr was the primary editor on this article and managed its editorial process and peer review in collaboration with the rest of the editorial team.

Publisher's note: Springer Nature remains neutral with regard to jurisdictional claims in published maps and institutional affiliations.

Methods

A Supplementary Protocol for the method described in the paper is available[21].

Microscopy setup. A sketch of the experimental setup is shown in Supplementary Note 2. The experimental setup consists of an inverted microscope (Olympus, IX73) with a mounted piezo translation stage (Physik Instrumente, P-733.3). The chrome structures are heated by a continuous wave laser at a wavelength of 808 nm (Pegasus Lasersysteme, PL.MI.808.300). The beam diameter is increased by a beam expander and sent to an acousto-optic deflector (Brimrose, 2DS-75-40-808) and a lens system to steer the laser focus in the sample plane. The deflected beam is focused by an objective lens (Olympus, ×100, 1.3 oil) to the sample plane (w_0 = 500-nm beam waist in the sample plane). The fluorescence of the ThT dye molecules is excited by a 445-nm laser (CNI, MDL-III-445-200), which is expanded and merged with the heating laser beam path by a pellicle beam splitter. The fluorescence excitation laser is focused to the back-focal plane to achieve homogeneous illumination in the trap center. Fluorescence is imaged by the same objective lens and a bandpass filter (Chroma, ET490/40) and a tube lens (500 mm) to an EMCCD (electron-multiplying charge-coupled device) camera (Andor iXon 3). A 750-nm short-pass filter (Thorlabs, FESH0750) is used to block back reflections from the heating laser. The dichroic beam splitter was selected according to the excitation, emission and heating laser wavelength (Omega Optical, XF2034). The acousto-optic deflector, as well as the piezo stage, are driven by an AD/DA (analog-digital/digital-analog) converter (ADwin-Gold II, Jäger Messtechnik). A LabVIEW program is used to record fluorescence images in real time and to control the AD/DA converter.

Ultraviolet lithography. The chrome structure was designed with AutoCAD and fabricated by means of ultraviolet lithography (Supplementary Note 1). First, glass coverslips were thoroughly cleaned with acetone and isopropyl and dried on a hotplate at 120 °C for 10 min. Subsequently, 100 µl of an adhesion promoter (MicroChemicals, TI PRIME Adhesion Promoter, 3,000 r.p.m., 30 s, followed by baking at 120 °C for 2 min on a hotplate) as well as 200 µl of a negative photoresist (MicroChemicals, AZ nLOF 2020, 3,000 r.p.m., 30 s, followed by a soft-bake at 110 °C for 60 s on a hotplate) were spin-coated successively onto the cover slides. Using an ultraviolet lithography system (Süss MicroTech, MJB4 Mask-Aligner) and a 3-inch photomask (Rose Fotomasken), the photoresist was exposed (66 mJ cm^{-2}, i-line) at regions of the desired chrome structures. The exposure was followed by a post-exposure bake at 110 °C for 60 s. The photoresist was then developed (MicroChemicals, AZ 326 MIF) for 60 s. Finally, a 30-nm chrome layer was thermally evaporated onto the coverslips and the non-depolymerized photoresist was stripped with a remover (MicroChemicals, TechniStrip NI555) in an ultrasonic bath for 30 min.

Fibril preparation. $A\beta_{40}$ fibrils were prepared by dissolving lyophilized $A\beta_{40}$ peptide (Core Unite Peptide, Leipzig University) in 25 mM phosphate buffer (pH 8.8) containing 150 mM NaCl at a concentration of 1 mg ml^{-1} followed by incubation for 12 h. For salt-dependent measurements 1-ml samples of the fibril stock solution were dialyzed against four different 25 mM phosphate buffer solutions with a 400-ml volume each: 10 mM NaCl (pH 7.4) and 1 mM NaCl (pH 6.1, pH 7.4 and pH 8.8) after 4 d of incubation. The molecular weight cut-off of the dialysis tube was 1,000 Da. The dialysis was performed for 4 h and the dialysis solution was changed after 2 h.

$A\beta_{42}$ fibrils were prepared by dissolving lyophilized $A\beta_{42}$ peptide (Core Unit Peptide, Leipzig University) in 25 mM phosphate buffer (150 mM NaCl, pH 9.2) at a concentration of 0.25 mg ml^{-1} followed by incubation for 4 d.

$pGlu_3$-$A\beta_{3-40}$ fibrils were prepared as described in ref. [17]. The lyophilized peptide (Core Unit Peptide, Leipzig University) was dissolved in 50 mM TRIS buffer (100 mM NaCl, pH 8.0) at a concentration of 0.1 mg ml^{-1} followed by incubation for 4 d. All peptide solutions were incubated at 37 °C while shaken at 450 r.p.m. (ThermoMixer, Eppendorf). The fibril stock solutions were then stored at room temperature until use.

Sample preparation. The sample consists of two glass coverslips (22 × 22 mm^2) confining a thin liquid film. One of the coverslips carries the chrome structures. First, the coverslips were thoroughly cleaned by rinsing successively with acetone, isopropyl and Milli-Q water and dried with a nitrogen gun. To prevent sticking of the fibrils, the glass surfaces were passivated with Pluronic F-127 (Sigma-Aldrich)[14]. To attain the adsorption of Pluronic F-127 in a brush-like configuration, the cleaned coverslips were rendered hydrophobic with a thin layer of polystyrene (PSS polymer, M_w = 88 kDa, PDI (polydispersity index) = 1.66). Next, 30 µl of 2% polystyrene in toluene was spin-coated at 8,000 r.p.m. onto the coverslips, resulting in a polystyrene layer thickness of about 100 nm. Subsequently, the coverslips are immersed in 1% Pluronic F-127 solution for 10 min. Thereafter, the coverslips were briefly dipped in Milli-Q water and dried with a nitrogen gun. Subsequently, the edges of the lower coverslip were covered with a thin layer of PDMS (polydimethylsiloxane) for sealing. The fibril solution used for the length-dependent experiments was prepared by diluting 5 µl of the fibril stock solution (pH 8.8, 150 mM NaCl) with 100 µl of Milli-Q water containing 0.1% Pluronic F-127 (ref. [22]) resulting in pH 8.4 (1 mM phosphate buffer) and 6 mM NaCl. For the buffer-dependent experiments, 5 µl of the dialyzed fibril stock solution were diluted with 100 µl of the corresponding buffer containing 0.1% Pluronic F-127. For growth experiments, 0.1 mg of the peptide monomers were added to the solution. Finally, 2 µl of a 1 mM ThT (Sigma-Aldrich) stock solution were added to attain a ThT concentration of about 20 µM (ref. [15]). Directly after preparation, 0.35 µl of the solution was pipetted in the middle of the lower coverslip (Supplementary Note 1). The upper coverslip was placed on top with the chrome structures facing down and the liquid spread between the glass coverslips. Depending on the wetted area, typically about 18 × 18 mm^2, the resulting thin liquid film was about 1 µm in height.

Reporting Summary. Further information on research design is available in the Nature Research Reporting Summary linked to this article.

Data availability

A dataset for demonstration can be downloaded at https://doi.org/10.5281/zenodo.1414296. The full dataset that supports the findings of this study is available from the corresponding author upon reasonable request.

Code availability

The source code and the files for the software used in this study are contained in the Supplementary Software, and a maintained version can be downloaded at https://github.com/molecular-nanophotonics/thermophoretic-trap-for-protein-aggregation-studies.

References

21. Fränzl, M. et al. *Protocol Exchange* https://doi.org/10.1038/protex.2019.031 (2019).
22. Luk, V. N., Mo, G. C. & Wheeler, A. R. *Langmuir* **24**, 6382–6389 (2008).

nature research

Corresponding author(s): NMETH-BC35910D

Reporting Summary

Nature Research wishes to improve the reproducibility of the work that we publish. This form provides structure for consistency and transparency in reporting. For further information on Nature Research policies, see Authors & Referees and the Editorial Policy Checklist.

Statistical parameters

When statistical analyses are reported, confirm that the following items are present in the relevant location (e.g. figure legend, table legend, main text, or Methods section).

n/a	Confirmed	
☐	☒	The exact sample size (*n*) for each experimental group/condition, given as a discrete number and unit of measurement
☐	☒	An indication of whether measurements were taken from distinct samples or whether the same sample was measured repeatedly
☒	☐	The statistical test(s) used AND whether they are one- or two-sided *Only common tests should be described solely by name; describe more complex techniques in the Methods section.*
☒	☐	A description of all covariates tested
☒	☐	A description of any assumptions or corrections, such as tests of normality and adjustment for multiple comparisons
☒	☐	A full description of the statistics including central tendency (e.g. means) or other basic estimates (e.g. regression coefficient) AND variation (e.g. standard deviation) or associated estimates of uncertainty (e.g. confidence intervals)
☒	☐	For null hypothesis testing, the test statistic (e.g. *F*, *t*, *r*) with confidence intervals, effect sizes, degrees of freedom and *P* value noted *Give P values as exact values whenever suitable.*
☒	☐	For Bayesian analysis, information on the choice of priors and Markov chain Monte Carlo settings
☒	☐	For hierarchical and complex designs, identification of the appropriate level for tests and full reporting of outcomes
☒	☐	Estimates of effect sizes (e.g. Cohen's *d*, Pearson's *r*), indicating how they were calculated
☐	☒	Clearly defined error bars *State explicitly what error bars represent (e.g. SD, SE, CI)*

Our web collection on statistics for biologists may be useful.

Software and code

Policy information about availability of computer code

Data collection	The data was collected using LabVIEW 2015 (Vision Development Module, MathScript RT Module). The FEM simulations were performed using COMSOL Multiphysics 5.2a (Heat Transfer Module)
Data analysis	For the data analysis Python scripts and Jupyter Notebooks were used. They are contained in the Supplementary Software 1 and a maintained version can be downloaded at https://github.com/Molecular-Nanophotonics/Thermophoretic-Trap-for-Protein-Aggregation-Studies

For manuscripts utilizing custom algorithms or software that are central to the research but not yet described in published literature, software must be made available to editors/reviewers upon request. We strongly encourage code deposition in a community repository (e.g. GitHub). See the Nature Research guidelines for submitting code & software for further information.

Data

Policy information about availability of data

All manuscripts must include a data availability statement. This statement should provide the following information, where applicable:

- Accession codes, unique identifiers, or web links for publicly available datasets
- A list of figures that have associated raw data
- A description of any restrictions on data availability

A sample dataset for demonstration is available at https://doi.org/10.5281/zenodo.1414296. The full dataset that supports the findings of this study is available from the corresponding author upon reasonable request.

Field-specific reporting

Please select the best fit for your research. If you are not sure, read the appropriate sections before making your selection.

☒ Life sciences ☐ Behavioural & social sciences ☐ Ecological, evolutionary & environmental sciences

For a reference copy of the document with all sections, see nature.com/authors/policies/ReportingSummary-flat.pdf

Life sciences study design

All studies must disclose on these points even when the disclosure is negative.

Sample size	The sample size N, i.e., the number of recorded images, was not predetermined. For all experiments the sample size was chosen large enough that statistical errors are minimal compared to the effect.
Data exclusions	We excluded data according to following pre-established criteria: Sample size N > 5000
Replication	The experimental findings of Fig. 2.a-b were obtained from independently prepared samples (new sample preparation for each buffer condition) thus directly demonstrating the reproducibility of the method. A length change has been observed for two different fibrils in Fig. 2c. A fibril fracture event in Fig. 2.e has be observed once.
Randomization	The randomization of the samples is intrinsic to the presented methods.
Blinding	Not relevant for this study as the work presents a trapping and image analysis scheme.

Reporting for specific materials, systems and methods

Materials & experimental systems

n/a	Involved in the study
☒	☐ Unique biological materials
☒	☐ Antibodies
☒	☐ Eukaryotic cell lines
☒	☐ Palaeontology
☒	☐ Animals and other organisms
☒	☐ Human research participants

Methods

n/a	Involved in the study
☒	☐ ChIP-seq
☒	☐ Flow cytometry
☒	☐ MRI-based neuroimaging